Modeling the Heterogeneity of Electrosensory Afferents in Electric Fish

Masterthesis

der Mathematisch-Naturwissenschaftlichen Fakultät
der Eberhard Karls Universität Tübingen

Erstkorrektor: Prof. Dr. Philipp Berens
Zweitkorrektor: Prof. Dr. Jan Benda

Lehrbereich für Neuroethologie

vorgelegt von
Alexander Mathias Ott
Abgabedatum: 21.09.2020

Eigenständigkeitserklärung

Hiermit erkläre ich, dass ich die vorgelegte Arbeit selbstständig verfasst habe und keine anderen als die angegebenen Quellen und Hilfsmittel benutzt habe.

Außerdem erkläre ich, dass die eingereichte Arbeit weder vollständig noch in wesentlichen Teilen Gegenstand eines anderen Prüfungsverfahrens gewesen ist.

Unterschrift	Ort, Datum

Contents

Not to forget: TODO

- update the colors in all plots to be consistent.
- make plot labels consistent (Units: in mV vs [mV])
- update number of cells / fish etc

1 Zusammenfassung

2 Abstract

3 Introduction

The environment of an organism holds important information that it needs to survive. Information about predators to avoid, food to find and potential mates. The ability to sense and process this information is of vital importance for any organism. At the same time the environment also contains a lot of information that is irrelevant to an organism. Barlow et al. (1961) suggested already that the sensory systems of an organism should be specialized to extract the information it needs while filtering out the noise and irrelevant information, to efficiently use the limited coding capacity of the sensory systems.

One interesting model system for questions adaptive signal processing is the electric fish *Apteronotus leptorhynchus* (Brown ghost knife fish). *A. leptorhynchus* generate a sinusoidal electric field with the electric organ in their tail enabling them to use active electroreception which they use to find prey and communicate with each other (Maciver et al. (2001), Zupanc et al. (2006)). The different use cases of this electric organ discharge (EOD) come with the necessity to detect a wide range of different amplitude modulations (AMs). Electrolocation of object in the surrounding water like small prey or rocks cause small low frequency AMs (Babineau et al., 2007). At the same time other electric fish can cause stronger and higher frequency AMs through interference between the electric fields and their communication signals like chirps, short increases in their EOD frequency (Zupanc et al., 2006). This means that the electroreceptors need to be able to encode a wide range of changes in EOD amplitude, in speed as well as strength. The EOD and its AMs are encoded by electroreceptor organs in the skin. *A. leptorhynchus* have two kinds of tuberous electrosensory organs: the T and P type units (Scheich et al., 1973). The T units (time coder) are strongly phase locked to the EOD and fire regularly once every EOD period. They encode the phase of the EOD in their spike timing. The P units (probability coders) on the other hand do not fire every EOD period. Instead they fire irregularly with a certain probability that depends on the EOD amplitude. That way they encode information about the EOD amplitude in their firing probability (Scheich et al., 1973). An example of the firing behavior of a P unit is shown in figure 1. When the fish's EOD is unperturbed P units fire every few EOD periods but they have a certain variability in their firing (fig. 1 B) and show negative correlation between successive interspike intervals (ISIs)(fig. 1 C). When presented with a step increase in EOD amplitude P units show strong adaption behavior. After a strong increase in firing rate reacting to the onset of the step, the firing rate quickly decays back to a steady state (fig. 1 D). When using different sizes of steps both the onset and the steady state response scale with its size and direction of the step (fig. 1 E).

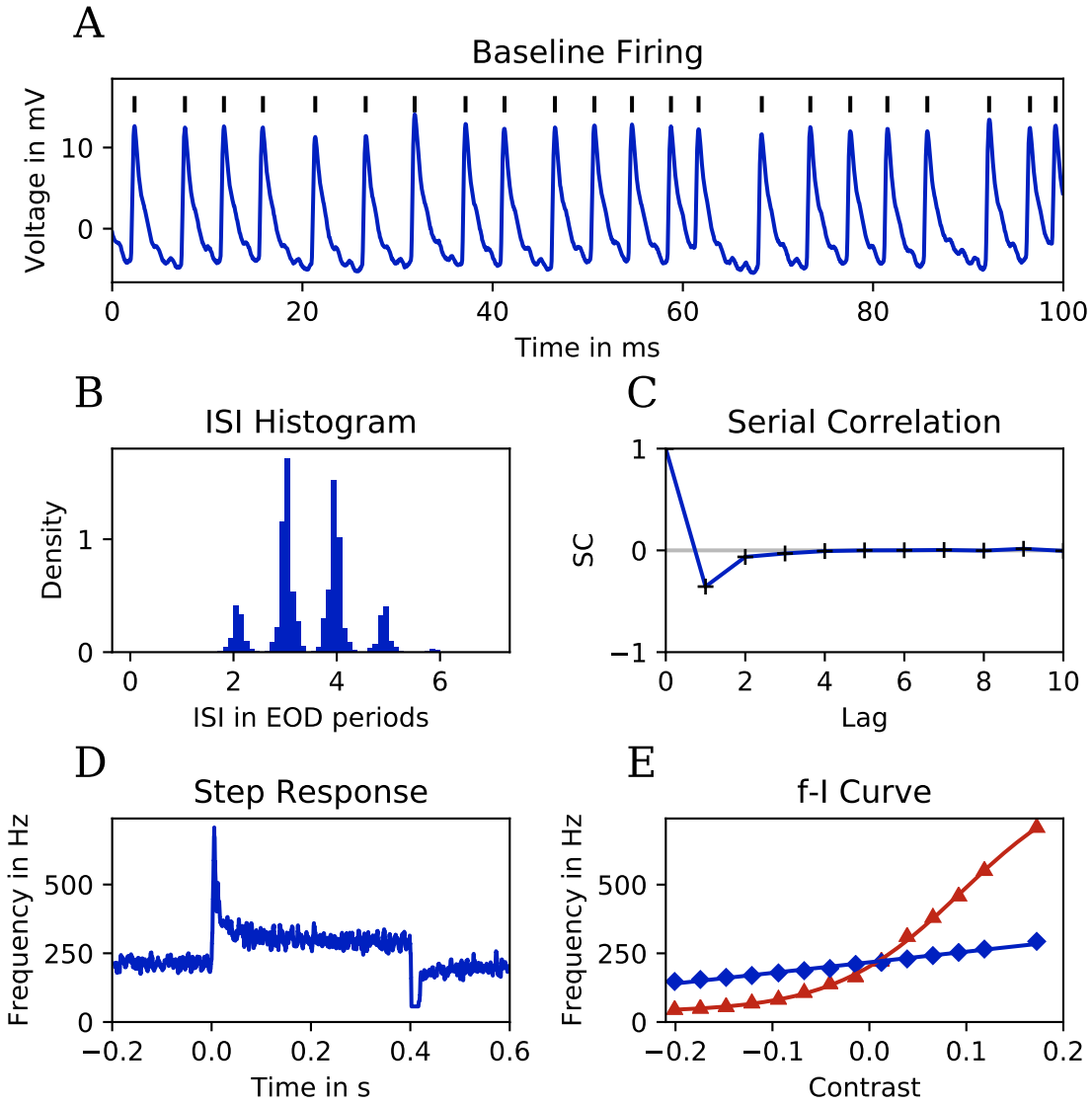

Figure 1: Example behavior of a P-unit with a high baseline firing rate and an EOD frequency of 744 Hz. **A**: A 100 ms voltage trace of the baseline recording with spikes marked by the black strokes. **B**: ISI histogram showing the phase locking of the P-unit firing to the EOD period. **C**: The serial correlation of the ISIs showing the negative correlation at lag one of most P-units. **D**: The response of the p-unit to a step increase in EOD amplitude. In (TODO: color) the averaged firing frequency (1/ISI) averaged over 10 trials. The P-unit strongly reacts to the onset of the stimulus but very quickly adapts to the new stimulus and then shows a reduced steady state response. **E**: The onset (TODO: color) and steady-state (TODO: color) f-I curves of the neuron display the dependence of both responses on the stimulus contrast. The lines are fits with a Boltzmann (eq.: 5) and a rectified line (6) for the onset and steady state f-I curve respectively.

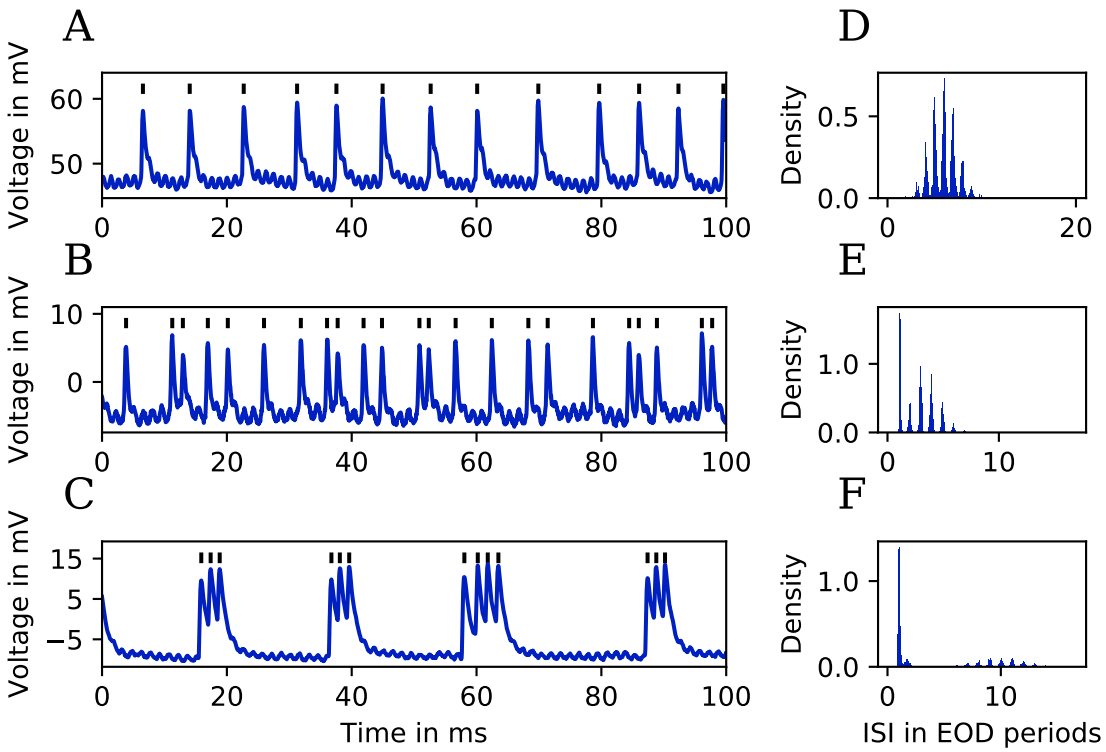

Figure 2: Variability in spiking behavior between P units under baseline conditions. **A**–**C** 100 ms of cell membrane voltage and **D**–**F** interspike interval histograms, each for three different cells. **A** and **D**: A non bursting cell with a baseline firing rate of 133 Hz (EODf: 806 Hz), **B** and **E**: A cell with some bursts and a baseline firing rate of 235 Hz (EODf: 682 Hz) and **C** and **F**: A strongly bursting cell with longer pauses between bursts (baseline rate of 153 Hz and EOD frequency of 670 Hz).

(TODO: heterogeneity more, bursts important for coding in other systems)

Furthermore show P-units a pronounced heterogeneity in their spiking behavior (fig. 2, Gussin et al. (2007)). This is an important aspect one needs to consider when trying to understand what and how information is encoded in the spike trains of the neuron (Padmanabhan and Urban (2010), Tripathy et al. (2013)). A single neuron might be an independent unit from all other neurons but through different tuning curves a full picture of the stimulus can be encoded in the population even when a single neuron only encodes a small feature space. This type of encoding is ubiquitous in the nervous system and is used in the visual sense for color vision, PLUS MORE... (TODO: refs labeled line vs summation code). Even though P units were already modeled based on a simple leaky integrate-and-fire neuron (Chacron et al., 2001) and conductance based (Kashimori et al., 1996) and well studied (Bastian (1981), Ratnam and Nelson (2000) Benda et al. (2005)). Up to this point there is no model that tries to cover the full breadth of heterogeneity of the P unit population. Having such a model could help shed light into the population code used in the electric sense and allow researchers gain a better picture how higher brain areas might process the information and get one step closer to the full path between sensory input and behavioral output. (TODO: viel wichtiger: das ist das perfekte modellsystem um die Kodierung in einer heterogenen population veon neuronen zu untersuchen. Relativ unabhaengig vom efish.)

4 Materials and Methods

(TODO: some transition from the introduction)

4.1 Cell recordings

The cell recordings for this master thesis were collected as part of other previous studies (Walz (2013), (Walz et al., 2014))(TODO: ref other studies) and the recording procedure is described there but will also be repeated below. The recordings of altogether 457 p-units were inspected. Of those 88 fulfilled basic necessary requirements: including a measurement of at least 30 seconds of baseline behavior and containing at least 7 different contrasts with each at least 7 trials for the f-I curve (see below fig. 4 B). After pre-analysis of those cells an additional 15 cells were excluded because of spike detection difficulties.

The 73 used cells came from 32 *Apteronotus leptorhynchus* (brown ghost knifefish). The fish were between 11–25 cm long (15.8 ± 3.5 cm) and their electric organ discharge (EOD) frequencies ranged between 601 and 928 Hz (753 ± 82 Hz). The sex of the fish was not determined.

The in vivo intracellular recordings of P-unit electroreceptors were done in the lateral line nerve. The fish were anesthetized with MS-222 (100-130 mg/l; PharmaQ; Fordingbridge, UK) and the part of the skin covering the lateral line just behind the skull was removed, while the area was anesthetized with Lidocaine (2%; bela-pharm; Vechta, Germany). The fish were immobilized for the recordings with Tubocurarine (Sigma-Aldrich; Steinheim, Germany, 25–50 μl of 5 mg/ml solution) and placed in the experimental tank (47 × 42 × 12 cm) filled with water from the fish's home tank with a conductivity of about 300μS/cm and the temperature was around 28°C. All experimental protocols were approved and complied with national and regional laws (files: no. 55.2-1-54-2531-135-09 and Regierungspräsidium Tübingen no. ZP 1/13 and no. ZP 1/16) For the recordings a standard glass mircoelectrode (borosilicate; 1.5 mm outer diameter; GB150F-8P, Science Products, Hofheim, Germany) was used. They were pulled to a resistance of 50–100 MΩ using Model P-97 from Sutter Instrument Co. (Novato, CA, USA) and filled with 1 M KCl solution. The electrodes were controlled using microdrives (Luigs-Neumann; Ratingen, Germany) and the potentials recorded with the bridge mode of the SEC-05 amplifier (npi-electronics GmbH, Tamm, Germany) and lowpass filtered at 10 kHz.

During the recording spikes were detected online using the peak detection algorithm from Todd and Andrews (1999). It uses a dynamically adjusted threshold value above the previously detected trough. To detect spikes through changes in amplitude the threshold was set to 50% of the amplitude of a detected spike while keeping the threshold above a minimum set to be higher than the noise level based on a histogram of all peak amplitudes. Trials with bad spike detection were removed from further analysis. The fish's EOD was recorded using two vertical carbon rods (11 cm long, 8 mm diameter) positioned in front of the head and behind its tail. The signal was amplified 200 to 500 times and bandpass filtered (3 − 1500 Hz passband, DPA2-FX, npi-electronics, Tamm, Germany). The electrodes were placed on iso-potential lines of the stimulus field to reduce the interference of the stimulus in the recording. All signals were digitized using a data acquisition board (PCI-6229; National Instruments, Austin TX, USA) at a sampling rate of 20–100 kHz (54 cells at 20 kHz, 20 at 100 kHz and 1 at 40 kHz)

The recording and stimulation was done using the ephys, efield, and efish plugins of the software RELACS (www.relacs.net). It allowed the online spike and EOD detection, pre-analysis and visualization and ran on a Debian computer.

4.2 Stimulus Protocols

The stimuli used during the recordings were presented from two vertical carbon rods (30 cm long, 8 mm diameter) as stimulus electrodes. They were positioned at either side of the fish parallel to its longitudinal axis. The stimuli were computer generated, attenuated and isolated (Attenuator: ATN-01M, Isolator: ISO-02V, npi-electronics, Tamm, Germany) and then send to the stimulus electrodes. For this work two types of recordings were made with all cells: baseline recordings and amplitude step recordings for the frequency-Intensity curve (f-I curve). The 'stimulus' for the baseline recording is purely the EOD field the fish produces itself with no external stimulus.

The amplitude step stimulus here is a step in EOD amplitude. The amplitude modulation (AM) is measured as a contrast. The contrast is calculated by dividing the EOD amplitude during the step by the normal EOD amplitude. To be able to cause a given AM in the fish's EOD, the EOD was recorded and multiplied with the modulation (see fig. 3). This modified EOD can then be presented at the right phase with the stimulus electrodes, causing constructive interference and adding the used amplitude modulation to the EOD (Fig. 3). This stimuli construction as seen in equation 1 works for any AM as long as the EOD of the fish is stable.

$$V_{Stim}(t) = EOD(t)(1 + AM(t)) \tag{1}$$

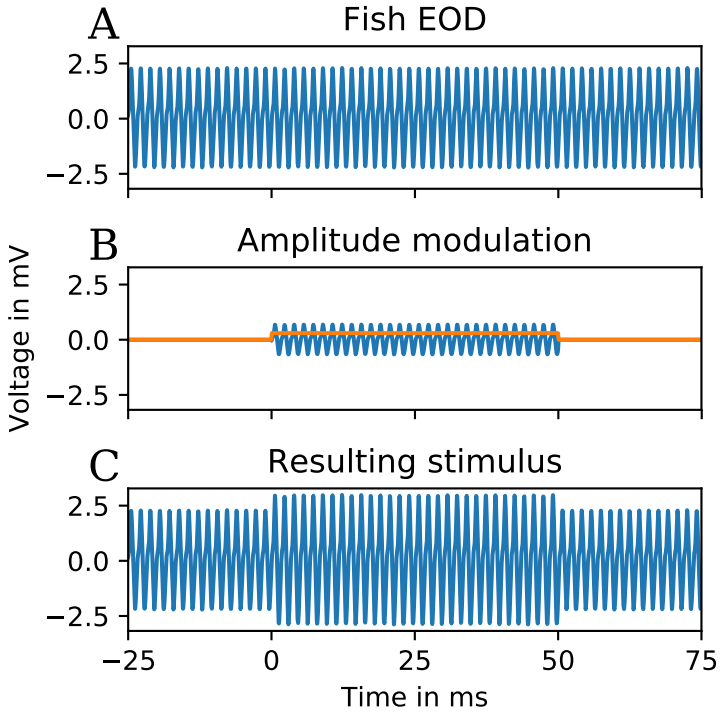

Figure 3: Example of the stimulus construction. At the top a recording of the fish's EOD. In the middle: EOD recording multiplied with the AM, with a step between 0 and 50 ms to a contrast of 30 % (marked in (TODO: color)). At the bottom the resulting stimulus trace when the AM is added to the EOD. (TODO: Umformulieren add figure labels A, B, C)

All step stimuli consisted of a delay of 0.2 s followed by a 0.4 s (n=68) or 1 s (n=7) long step and a 0.8 s long recovery time. The contrast range measured was for the most cells 80–120% of EOD amplitude. Some cells were measured in a larger range up to 20–180%. In the range at least 7 contrasts were measured with at least 7 trials, but again many cells were measured with more contrasts and trials. The additionally measured contrasts were used for the model if they had at least 3 trials.

4.3 Cell Characteristics

The cells were characterized by ten parameters: 6 for the baseline and 4 for the f-I curve. For the baseline the mean firing rate was calculated by dividing the number of spikes in the recording by the recording time. Then the set of all interspike intervals (ISI) T was computed and further parameters were calculated from it.

The coefficient of variation

$$CV = \frac{STD(T)}{\langle T \rangle} \tag{2}$$

is defined as the standard deviation (STD) of T divided by the mean ISI, see equation 2 with angled brackets as the averaging operator.

The vector strength (VS) is a measure of how strong the cell locks to a phase of the EOD. It was calculated as seen in Eq. 3, by placing each spike on a unit circle depending on the relative spike time t_i of how much time has passed since the start of the current EOD period in relation to the EOD period length. This set of vectors is then averaged and the absolute value of this average vector describes the VS. If the VS is zero the spikes happen equally in all phases of the EOD while if it is one all spikes happen at the exact same phase of the EOD.

$$vs = |\frac{1}{n}\sum_{n} e^{iwt_i}| \tag{3}$$

The serial correlation with lag k (SC_k) of T is a measure how the ISI T_i (the i-th ISI) influences the T_{i+k} the ISI with a lag of k intervals. This is calculated as,

$$SC_k = \frac{\langle (T_i - \langle T \rangle)(T_{i+k} - \langle T \rangle) \rangle}{\sqrt{\langle (T_i - \langle T \rangle)^2 \rangle}\sqrt{\langle (T_{i+k} - \langle T \rangle)^2 \rangle}} \tag{4}$$

with the angled brackets again the averaging operator.

Finally the ISI-histogram was calculated within a range of 0–50 ms and a bin size of 0.1 ms. The burstiness was calculated as the percentage of ISI smaller than 2.5 EOD periods multiplied by the average ISI. This gives a rough measure of how how often a cell fires in the immediately following EOD periods compared to its average firing frequency.

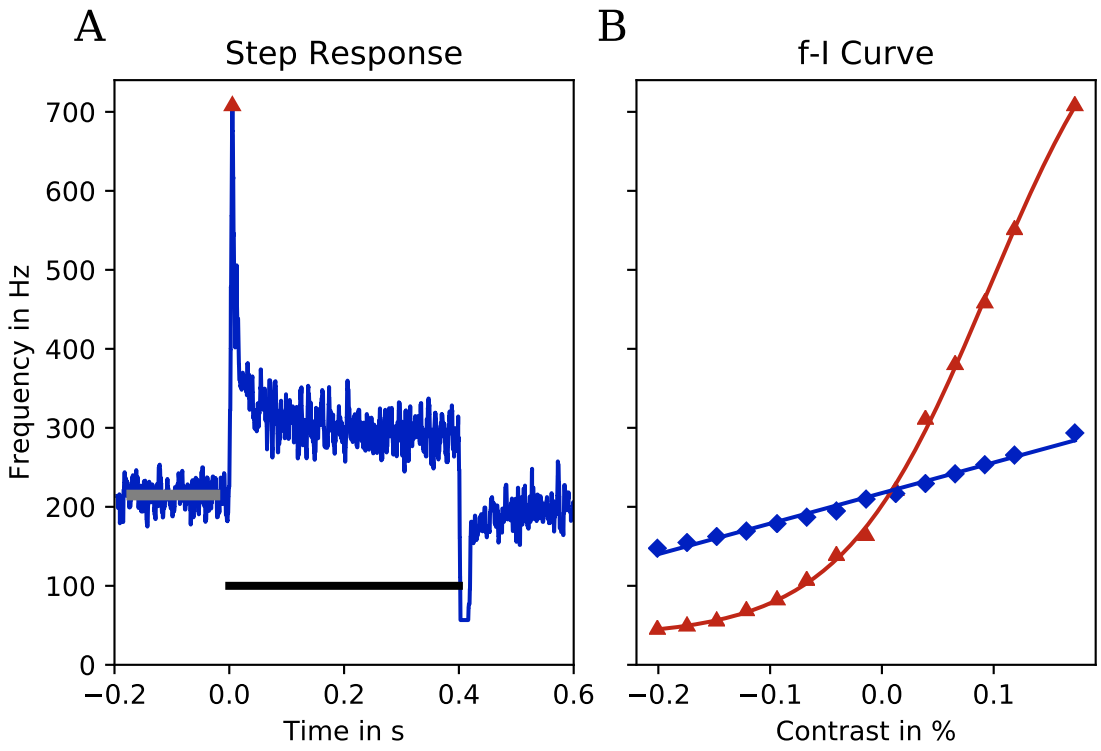

Figure 4: **A**: The averaged response of a cell to a step in EOD amplitude. The step of the stimulus is marked by the back bar. The detected values for the onset (f_0) and steady-state (f_∞) response are marked in (TODO: color). f_0 is detected as the highest deviation from the mean frequency before the stimulus while f_∞ is the average frequency in the 0.1 s time window, 25 ms before the end of the stimulus. **B**: The fi-curve visualizes the onset and steady-state response of the neuron for different stimuli contrasts. In (TODO: color) the detected onset responses and the fitted Boltzmann, in (TODO: color) the detected steady-state response and the linear fit.

As already mentioned in the introduction, p-units react to a step in EOD amplitude with a strong onset response decaying back to a steady state response (fig. 4 A). This adaption behavior of the cell was characterized by the f-I curve measurements. First the ISI frequency trace for each stimulus was calculated. The ISI frequency of a time point t is defined as $1/T_i$ with T_i the ISI the time point t falls into. This gives a frequency trace starting with the first spike and ending at the last spike. For further analysis all trials of a specific contrast were averaged over the trials with the resolution of the sampling rate. This results in a trial-averaged step response for each contrast as illustrated in figure 4 A. In this firing frequency trace the baseline frequency, the onset f_0 and steady-state f_∞ response were detected. The baseline frequency was measured as the mean of the firing frequency 25 ms after recording start up to 25 ms before the stimulus start. f_0 was then defined as the largest deviation from the baseline frequency, within the first 25 ms after stimulus onset. If there was no deviation farther than the minimum or maximum before the stimulus start, then the average frequency in that 25 ms time window was used. This approximation made the detection of f_0 more stable for small contrasts and trials with high variation. The f_∞ response was estimated as the average firing frequency in the 100 ms time window ending 25 ms before the end of the stimulus (fig. 4 A). Afterwards a Boltzmann:

$$f_0(I) = (f_{max} - f_{min})(1/(1 + e^{-k*(I-I_0)})) + f_{min} \tag{5}$$

was fitted to the onset response and a rectified line:

$$f_\infty(I) = \lfloor mI + c \rfloor_0 \tag{6}$$

(with $\lfloor x \rfloor_0$ the rectify operator) was fitted to the steady-state responses (fig. 4 B).

4.4 Leaky Integrate and Fire Model

The above described cell characteristics need to be reproduced by a simple and efficient model to be able to simulate bigger populations in a reasonable time. The model used in this thesis follows these equations:

$$\tau_m \frac{dV}{dt} = -V + I_{Bias} + \alpha V_{dend} - I_A + \sqrt{2D}\frac{\xi}{\sqrt{\Delta t}} \tag{7}$$

$$\tau_A \frac{dI_A}{dt} = -I_A + \Delta_A \sum \delta(t) \tag{8}$$

$$\tau_{dend} \frac{dV_{dend}}{dt} = -V_{dend} + \lfloor V_{stim} \rfloor_0 \tag{9}$$

Equation 7 describes the leaky dynamics of the membrane voltage with τ_m the membrane time constant, I_{Bias} a bias current, α the cell specific gain factor for V_{dend} the input voltage coming from the dendrite. $\sqrt{2D}$ is the strength of the normal distributed noise ξ. I_A is an adaption current with the dynamics of equation 8. τ_A is the time constant of the adaption, Δ_A its strength and $\delta(t)$ is the spike train of the cell. Equation 9 shows the dynamics of the synapse and dendrite with τ_{dend} the time constant of the dendrite and $\lfloor V_{stim} \rfloor_0$ the rectified stimulus given. Finally the model also includes a refractory period t_{ref}, not shown in above equations, that keeps the membrane voltage V at zero for its duration.

To arrive at this model the simplest commonly used neuron model the perfect integrate-and-fire (PIF) model was stepwise extended. The PIF's voltage can be described in one equation: $\tau_m \frac{dV}{dt} = \frac{I}{R_m}$ with I the stimulus current, R_m the membrane resistance and a voltage threshold V_θ. In this model I is integrated and when this threshold θ is reached the voltage is reset to zero and a spike is recorded (see fig. 5 PIF). The model is useful for basic simulations but cannot reproduce the richer behavior of the p-units, as it has no memory of previous spikes so it cannot show any adaption behavior and it is also very strongly locked to its limit cycle producing very constant ISI, not allowing the firing flexibility of the p-units.

The next slightly more complex model is the leaky integrate-and-fire (LIF) model:

$$\tau_m \frac{dV}{dt} = -V + IR_m \tag{10}$$

As the name suggests it adds a leakage current to the PIF (fig. 5 LIF). The leakage current adds sub threshold behavior to the model and allows for some more flexibility in suprathresold firing but it is still not flexible enough and cannot reproduce the adaption.

To reproduce the adaption behavior the model needs some form of memory of previous spikes. There are two main ways this can be added to the model as an adaptive current or a dynamic threshold. The biophysical mechanism of the adaption in p-units is unknown because the cell bodies are not accessible for intra-cellular recordings. Following the results of Benda et al. (2010) a negative adaptive current was chosen, because the dynamic threshold causes divisive adaption instead of the subtractive adaption of p-units seen in Benda et al. (2005). This results in an leaky integrate-and-fire model with adaption current (LIFAC) (fig. 5 LIFAC). The added adaptive current follow the dynamics:

$$\tau_A \frac{dI_A}{dt} = -I_A + \Delta_A \sum \delta(t) \tag{11}$$

and gets subtracted from the input current I of of the voltage dynamics eq. 10. It is modeled as an exponential decay with the time constant τ_A and an adaption strength Δ_A. Δ_A is multiplied with the sum of spikes t_i in the spike train ($\delta(t_i)$) of the model cell. For the simulation using the Euler integration this results in an increase of I_A by $\frac{\Delta_A}{\tau_A}$ at every time step where a spike is recorded. (TODO: image of model simulation with voltage adaption and spikes using the toy model?) The input current I from equation 10 is a sum of those two currents and an additional bias current I_{Bias} that is needed to adjusts the cells spontaneous spiking:

$$I = \alpha I_{Input} - I_A + I_{Bias} \tag{12}$$

Note that in this p-unit model all currents are measured in mV because, as mentioned above, the cell body is not accessible for intra-cellular recordings and as such the membrane resistance R_m is unknown (TODO: ref mem res p-units). The input current I_{Input} is the current of the stimulus, an amplitude modulated sine wave mimicking the frequency EOD. This stimulus is then rectified to model the receptor synapse and low-pass filtered with a time constant of τ_{dend} to simulate the low-pass filter properties of the dendrite (fig. 6) according to:

$$\tau_{dend}\frac{dV_{dend}}{dt} = -V_{dend} + \lfloor I_{Input} \rfloor_0 \tag{13}$$

Afterwards it is multiplied with α a cell specific gain factor. This gain factor has the unit of cm because the I_{Input} stimulus represents the EOD with a unit of mV/cm.

Finally, noise and an absolute refractory period were added to the model. The noise ξ is drawn from a Gaussian noise distribution and divided by $\sqrt{\Delta t}$ to get a noise which autocorrelation function is independent of the simulation step size Δt. The implemented form of the absolute refractory period t_{ref} keeps the model voltage at zero for the duration of t_{ref} after a spike. This gives us the full model described in equations 7–9.

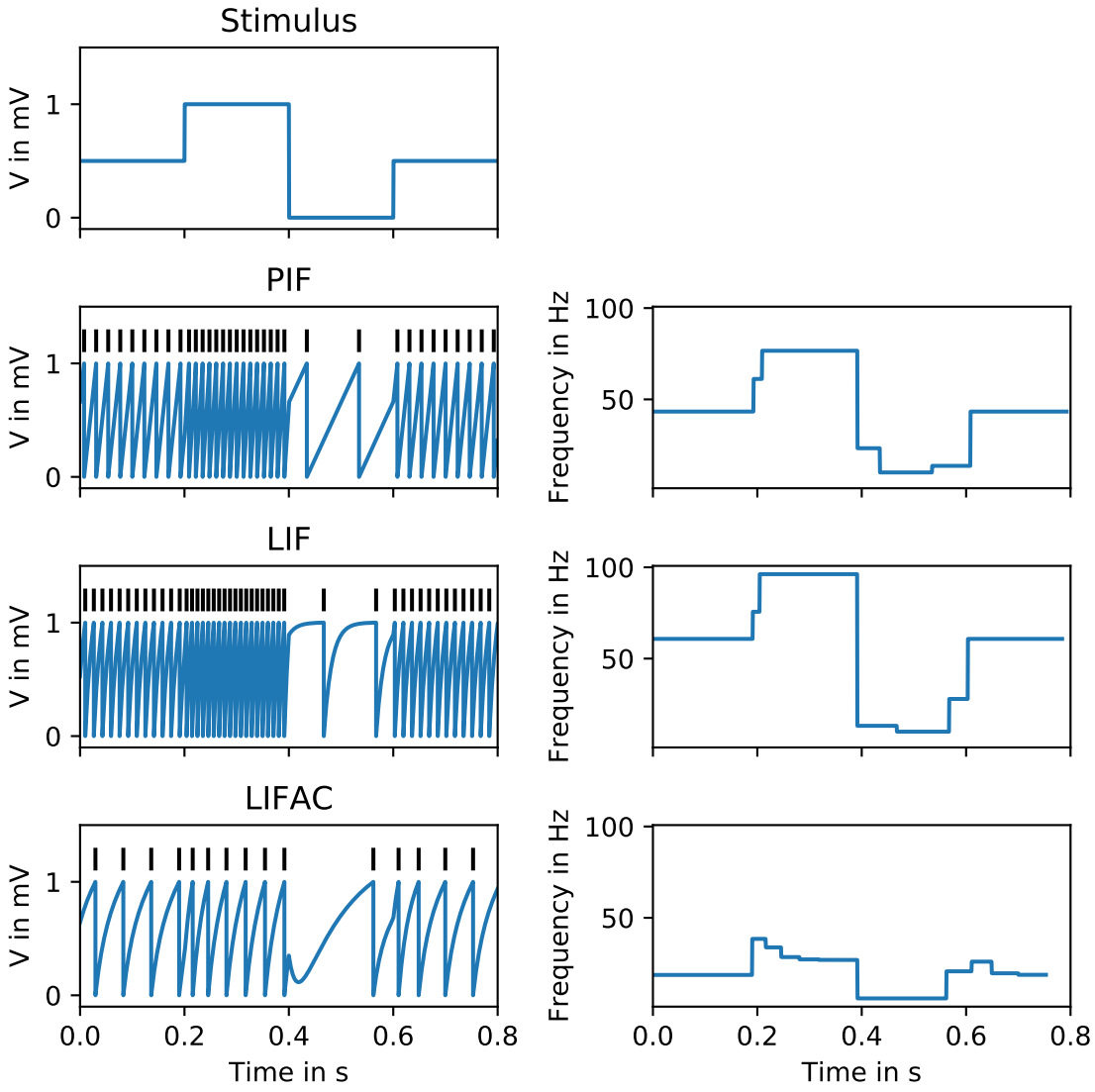

Figure 5: Comparison of different simple models normed to a spontaneous firing rate of 10 Hz stimulated with a step stimulus. In the left column y-axis in mV in the right column the y-axis shows the frequency in Hz. PIF: Shows a continuously increasing membrane voltage with a fixed slope and as such constant frequency for a given stimulus strength. LIF: Approaches a stimulus dependent membrane voltage steady state exponentially Also has constant frequency for a fixed stimulus value. LIFAC: Exponentially approaches its new membrane voltage value but also shows adaption after changes in the stimulus the frequency takes some time to adapt and arrive at the new stable value.

Together this results in the dynamics seen in equations 7–9.

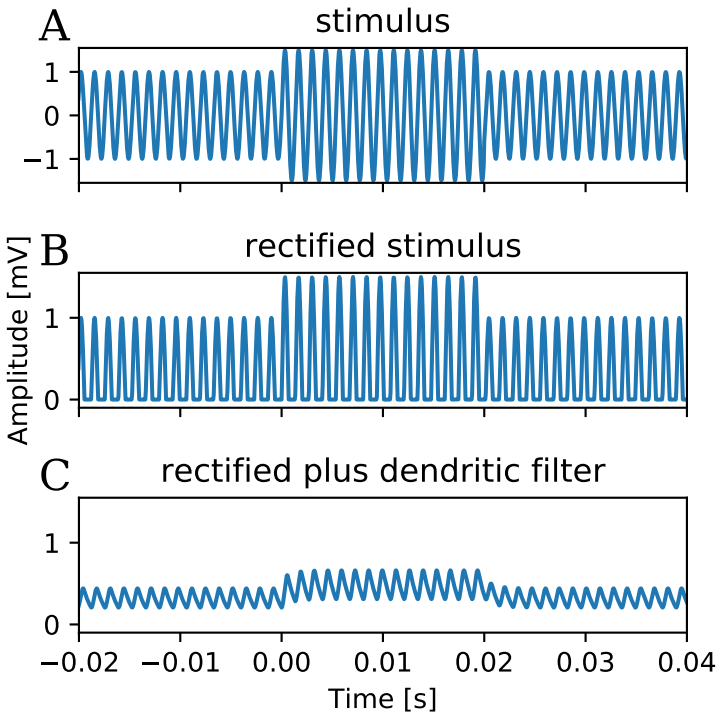

Figure 6: The stimulus modification in the model. The fish's EOD is simulated with a sin wave. It is rectified at the synapse and then low-pass filtered in the dendrite.

parameter	explanation	unit
α	stimulus scaling factor	[cm]
τ_m	membrane time constant	[ms]
I_{Bias}	bias current	[mV]
$\sqrt{2D}$	noise strength	[mV$\sqrt{\text{s}}$]
τ_A	adaption time constant	[ms]
Δ_A	adaption strength	[mVms]
τ_{dend}	time constant of dendritic low-pass filter	[ms]
t_{ref}	absolute refractory period	[ms]

Table 1: Overview about all parameters of the model that are fitted.

4.5 Fitting of the Model

The full model has, as described above, eight parameters that need to be fitted so it can reproduce the behavior of the cell. During the fitting and the analysis all models were integrated with at time step of 0.05 ms. The stimuli described in the stimulus protocols section above were recreated for the stimulation of the model during the fitting process. The pure fish EOD was approximated by a simple sine wave of the appropriate frequency, but it was decided to keep the amplitude of the sine wave at one to make the models more comparable. Changes in the amplitude can be compensated for by changing the input scaling factor so there is no qualitative difference.

During the fitting the baseline stimulus was simulated 3 times with 30 s each and the step stimuli were simulated with a delay, step duration and recovery time of each 0.5 s. The contrasts were the same as in the cell recordings. The step stimuli for the different

contrasts were each repeated 8 times. The simulated data was analyzed in the same way as the cells (see above).

The error function was constructed from both the baseline characteristics: VS, CV, SC, ISI-histogram and burstiness and the f-I curve: the detections of f_{inf} and f_0 responses for each contrast, the slope of the linear fit into the f_{inf} and the frequency trace of one step response.

The error of the VS, CV, SC, and burstiness was calculated as the scaled absolute difference:

$$err_i = c_i |x_i^M - x_i^C| \tag{14}$$

with x_i^M the model value for the characteristic i, x_i^C the corresponding cell value and c_i a scaling factor that is the same for all cells but different between characteristics. The scaling factor was used to make all errors a similar size. They are listed in table 2.

The error for the slope of the f_{inf} fit was the scaled relative difference:

$$err_i = c_i |1 - ((x_i^M - x_i^C)/x_i^C)| \tag{15}$$

For the f_{inf} and f_0 responses the average scaled difference off all contrasts was taken and finally the error for the ISI-histogram and the step-response was calculated with a mean-square error. For the histogram over all bins but for the step response only the first 50 ms after stimulus onset as an error for the adaption time constant.

$$err_i = c_i(\langle (x_i^M - x_i^C)^2 \rangle) \tag{16}$$

All errors were then summed up for the full error. The fits were done with the Nelder-Mead algorithm of scipy minimize (Gao and Han, 2012). All model variables listed above in table 1 were fit at the same time except for I_{Bias}. I_{Bias} was determined before each fitting iteration and set to a value giving the correct baseline frequency within 2 Hz.

behavior	scaling factor
vector strength	100
coefficient of variation	20
serial correlation	10
ISI-histogram	1/600
f_0 detections	0.1
f_∞ detections	1
f_∞ slope	20
f_0 step response	0.001

Table 2: Scaling factors for fitting errors.

(TODO: Fitting more in detail number of start parameters the start parameters themselves)

(TODO: explain removal of bad models! Filter criteria how many filtered etc.)

(TODO: explain how to draw random models from fitted model parameters! here probably?)

5 Results

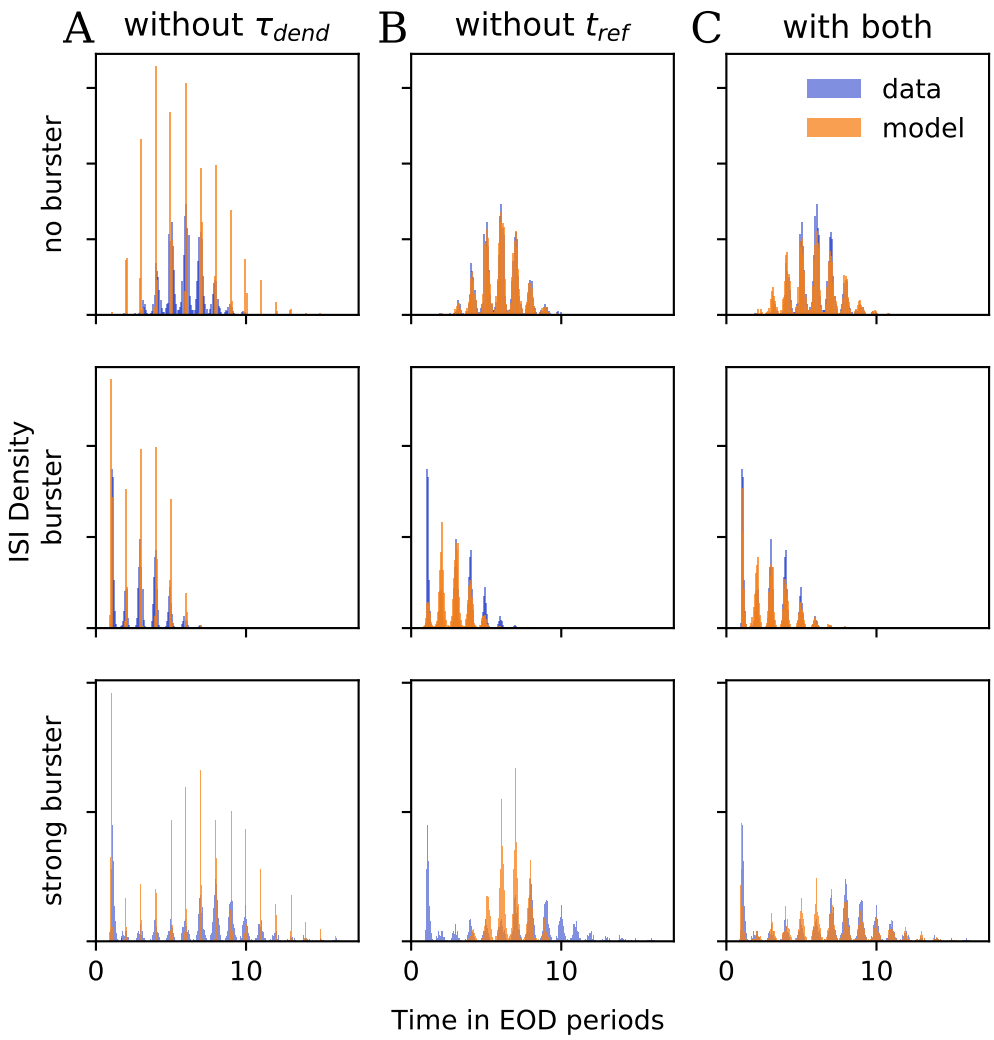

Figure 7: Effect of the dendritic filter and the refractory period on baseline firing. In each row data (blue) and model fits (orange) to three example cells are shown that differ in their burstiness as indicated on the left. (TODO: Top: cell 2012-xxx, r=z Hz, b=y; center: cell 2014-xxx, r= b=...; bottom ...) A: Without dendritic filter (τ_{dend}) the spikes are too strongly locked to the EOD, resulting in very high vector strength and too narrow peaks in the baseline ISIH. B: Without refactory period (t_{ref}) the model cannot capture burstiness. While this is no problem for the non-bursting cell (top), the peak in the ISIH at one EOD period cannot be reproduced without refacory period. C: with both the dendritic filter and the refracory period ISIhs can be faithfully reproduced for all three cells.

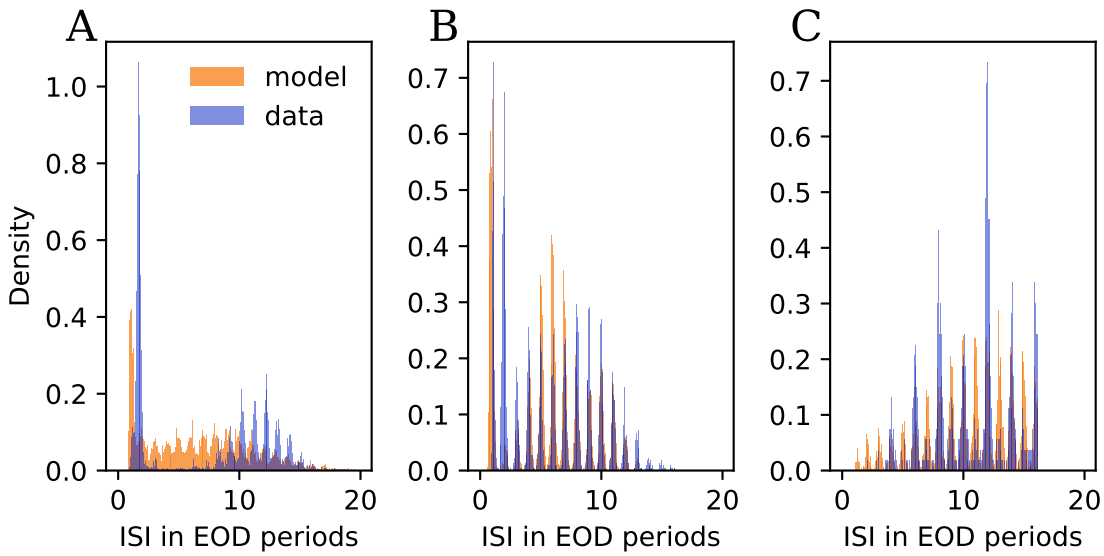

Figure 8: (TODO: Add pointer arrows in plot?) Problem cases in which the model ISI histogram wasn't fit correctly to the cell. ISI histograms of different cells ((TODO: color)) and their corresponding model ((TODO: color)). **A**: Strongly bursting cell with large pauses between bursts, where the model doesn't manage to reproduce the long pauses. **B**: Bursting cell with a high probability of firing in the first and second following EOD period. Here the model can't reproduce the high probability on the second following EOD period. **C**: Cell with a higher order structure (TODO: ??) in its ISI histogram. It only has a high firing probability every second EOD period which is also not represented in the model.

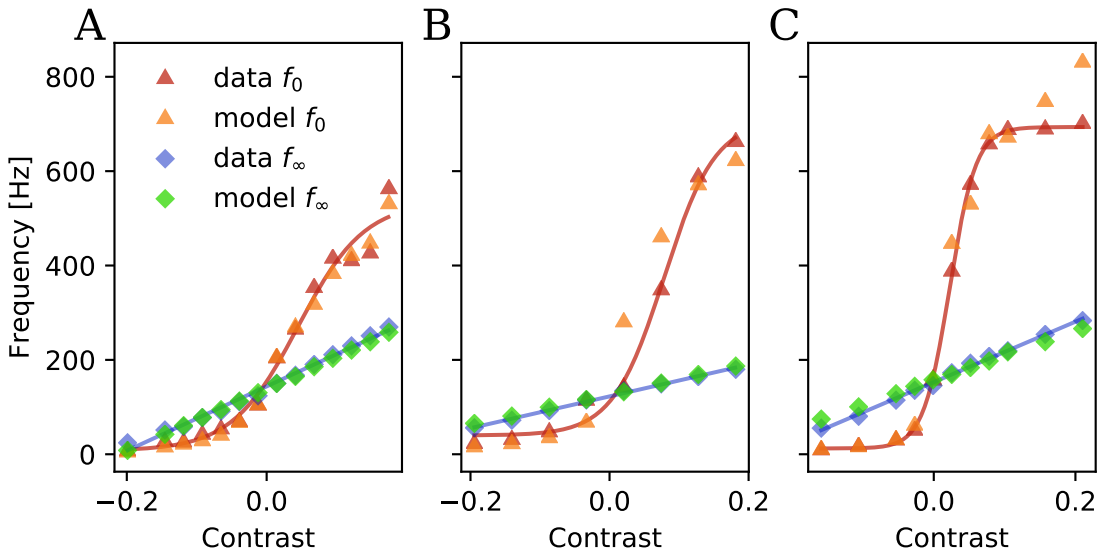

Figure 9: Good fit examples of the f-I curve. **A**–**C**: Three cells with different response patterns which are all well matched by their models. (TODO: Color explanation)

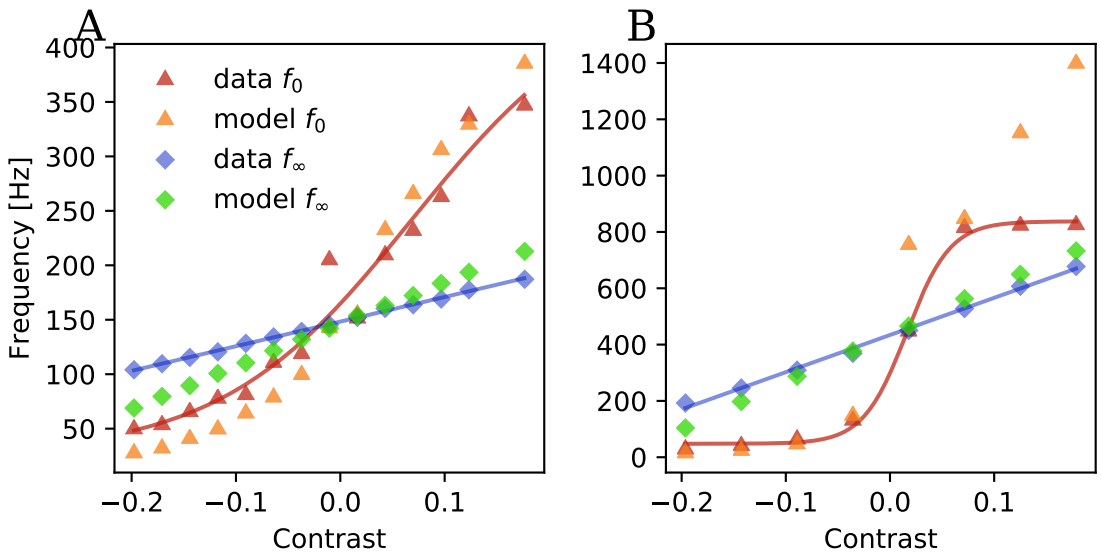

Figure 10: Examples of bad fits of the f-I curve. **A**–**C**: Different cells. (TODO: Color explanation). **A**: model that did not fit the negative contrast responses of the f_0 response well but was successful in the positive half. It also was not successful in the f_∞ response and shows a wrong slope. **B**: A fit that was successful for the lower f_0 response but overshoots the limit of the cell and fires too fast for high positive contrasts. It also has a slightly wrong f_∞ response slope.

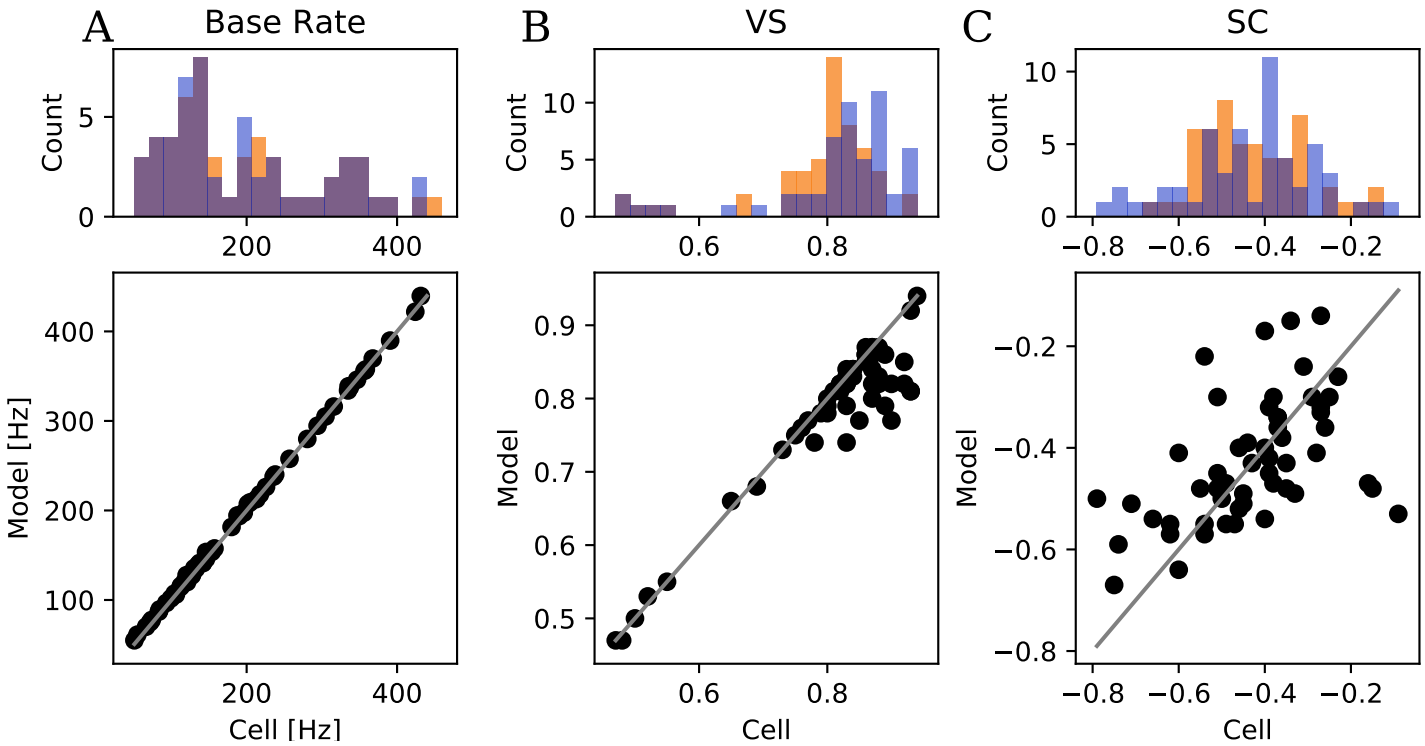

Figure 11: Comparison of the cell behavior and the behavior of the corresponding fit: **A** baseline firing rate, **B** vector strength (VS) and **C** serial correlation (SC). The histograms compare the distributions of the cell ((TODO: color)) and the model ((TODO: color)). Below (TODO: what is this plot called) In grey the line on which cell and model values are equal. **A**: The baseline firing rate of the cell and the model. The base rate agrees near perfectly as it is set to be equal within a margin of 2 Hz during the fitting process. **B**: The vector strength agrees well for most cells but if the cells have a vector strength above 0.8 the probability increases for the models to show often a weaker VS than the cell. **C**: Comparison of the SC with lag 1. Here the models cluster more strongly and don't show quite the same range like the cells do. Models of cells with a strongly negative SC often have a weaker negative SC while the models in the opposite case show too strong negative correlations. In general is the fitting of the SC a lot more variable than the precise fitting of the VS.

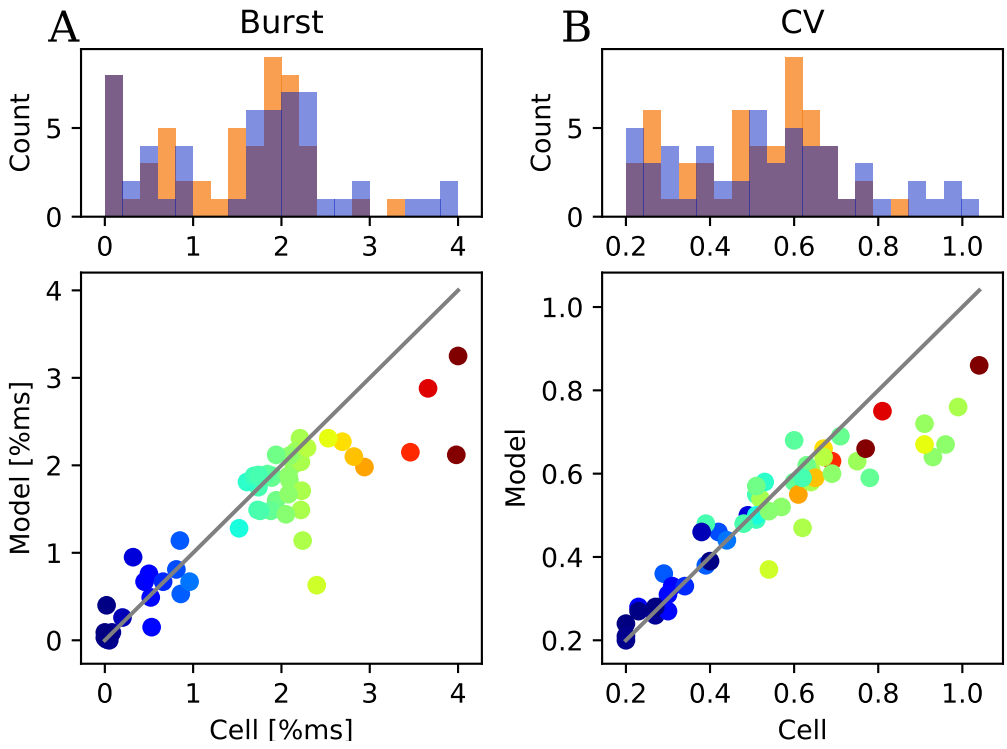

Figure 12: Comparison of the cell behavior and the behavior of the corresponding fit: **A** burstiness, **B** coefficient of variation (CV). **A**: The model values for the burstiness agree well with the values of the model but again show a tendency that the higher the value of the cell the more the model value is below it. **B**: The CV also shows the problem of the burstiness but the values drift apart more slowly starting around 0.6.

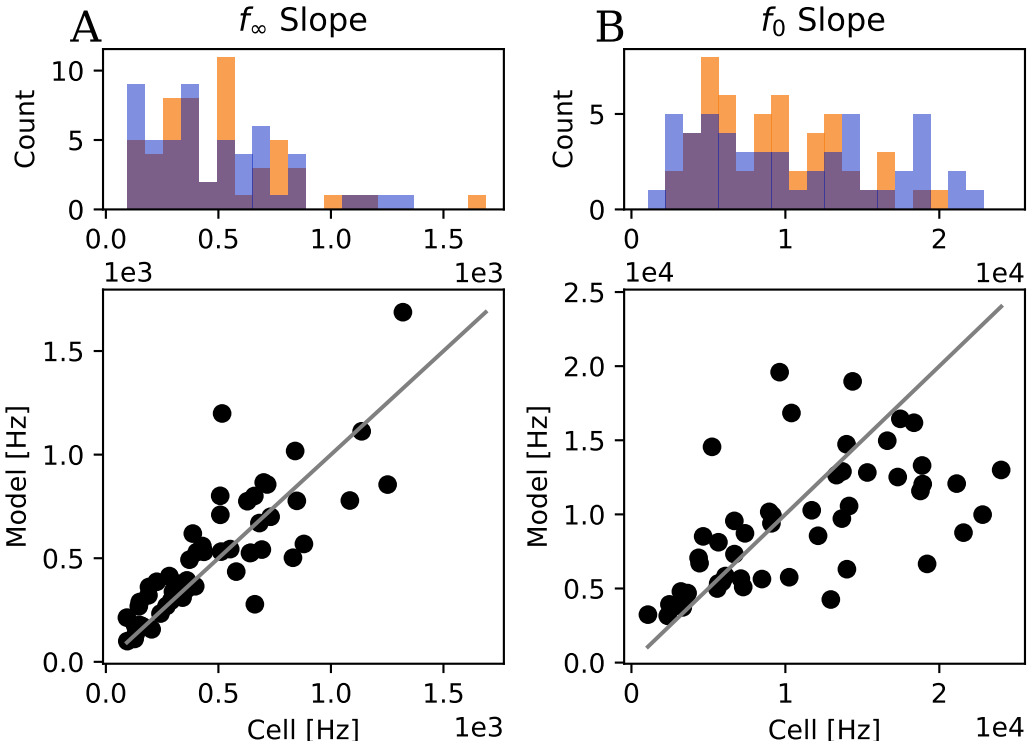

Figure 13: Comparison of the cell behavior and the behavior of the corresponding fit: **A** steady state f_∞ and **B** onset f_0 response slope. In grey the line on which cell and model values are equal. (TODO: how many) value pairs from **B** lie outside of the shown area. They had slopes between (TODO:). In **A** the f_∞ slope pairs. Cell and models show good agreement with a low scattering in both direction. **B** The f_0 values show a higher spread and for steeper slopes the models have more often too flat slopes.

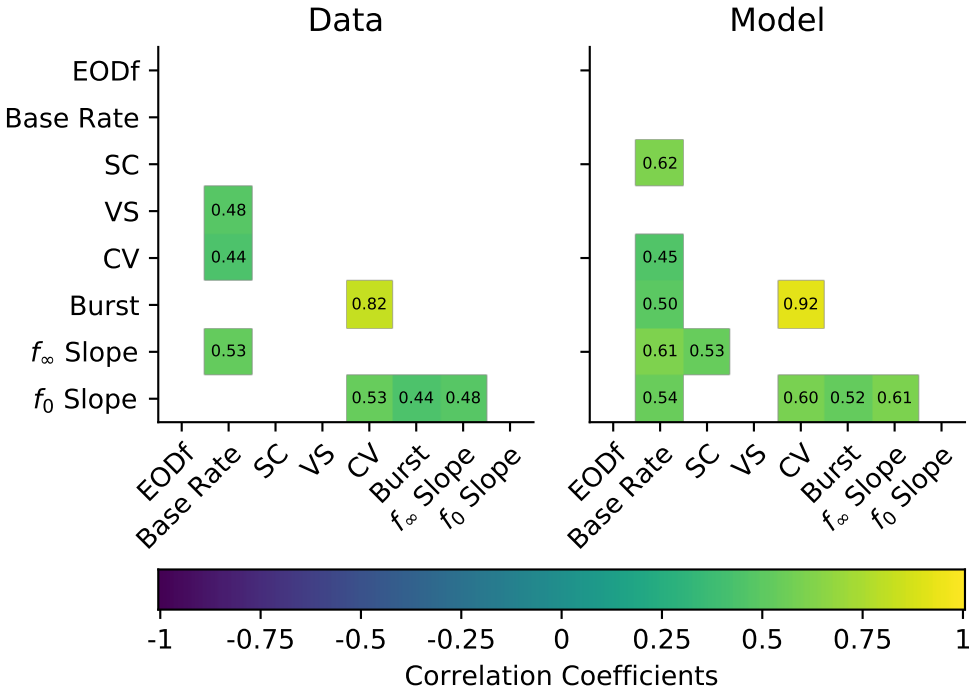

Figure 14: Significant correlations between the behavior variables in the data and the fitted models $p < 0.05$ (Bonferroni corrected). The models contain all the same correlations as the data except for the correlation between the baseline firing rate and the VS, but they also show four additional correlations not seen within the cells: bursting - base rate, SC - f_∞ slope, f_0 slope - base rate, SC - base rate.

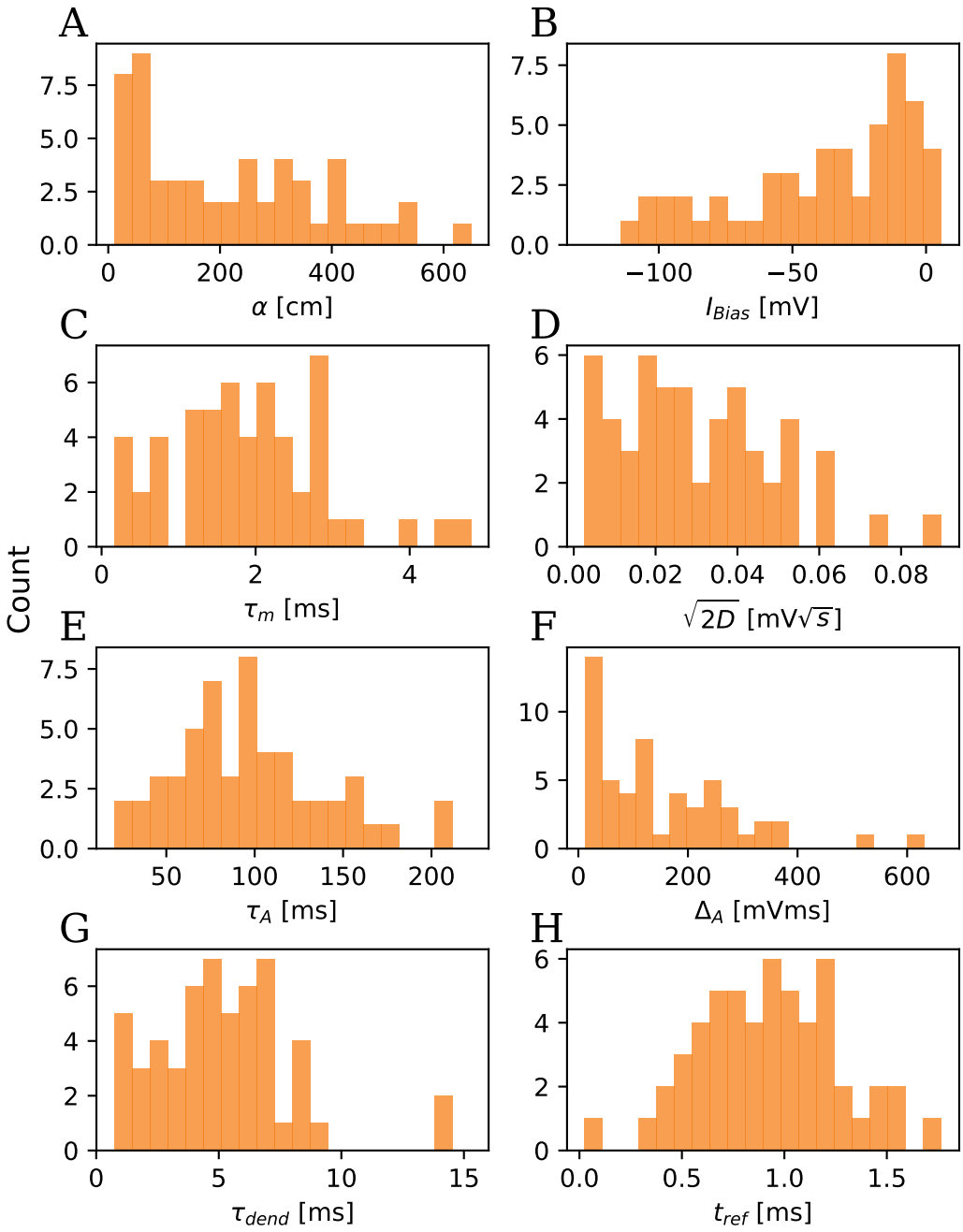

Figure 15: Distributions of all eight model parameters. **A**: input scaling α, **B**: Bias current I_{Bias}, **C**: membrane time constant τ_m, **D**: noise strength $\sqrt{2D}$, **E**: adaption time constant τ_A, **F**: adaption strength Δ_A, **G**: time constant of the dendritic low pass filter τ_{dend}, **H**: refractory period t_{ref}

(TODO: image with rescaled time parameters to 800 Hz, add to above figure?)

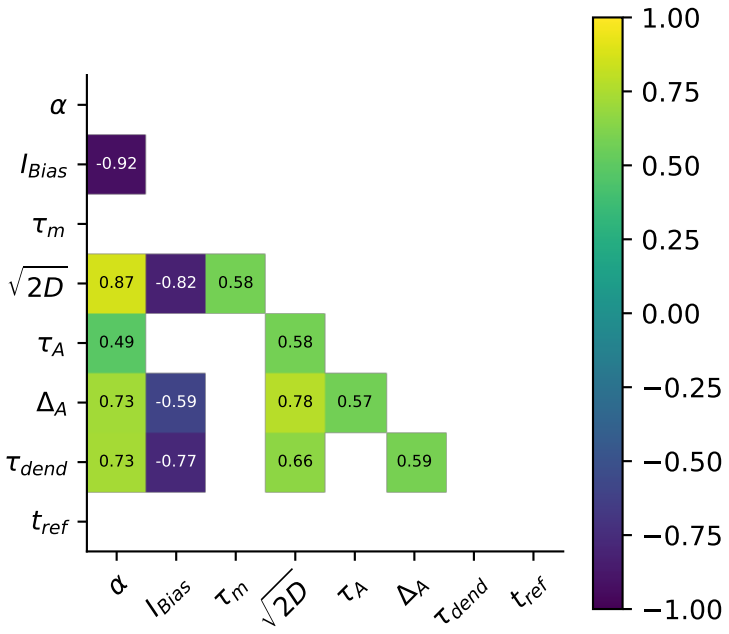

Figure 16: Significant correlations between model parameters $p < 0.05$ (Bonferroni corrected).

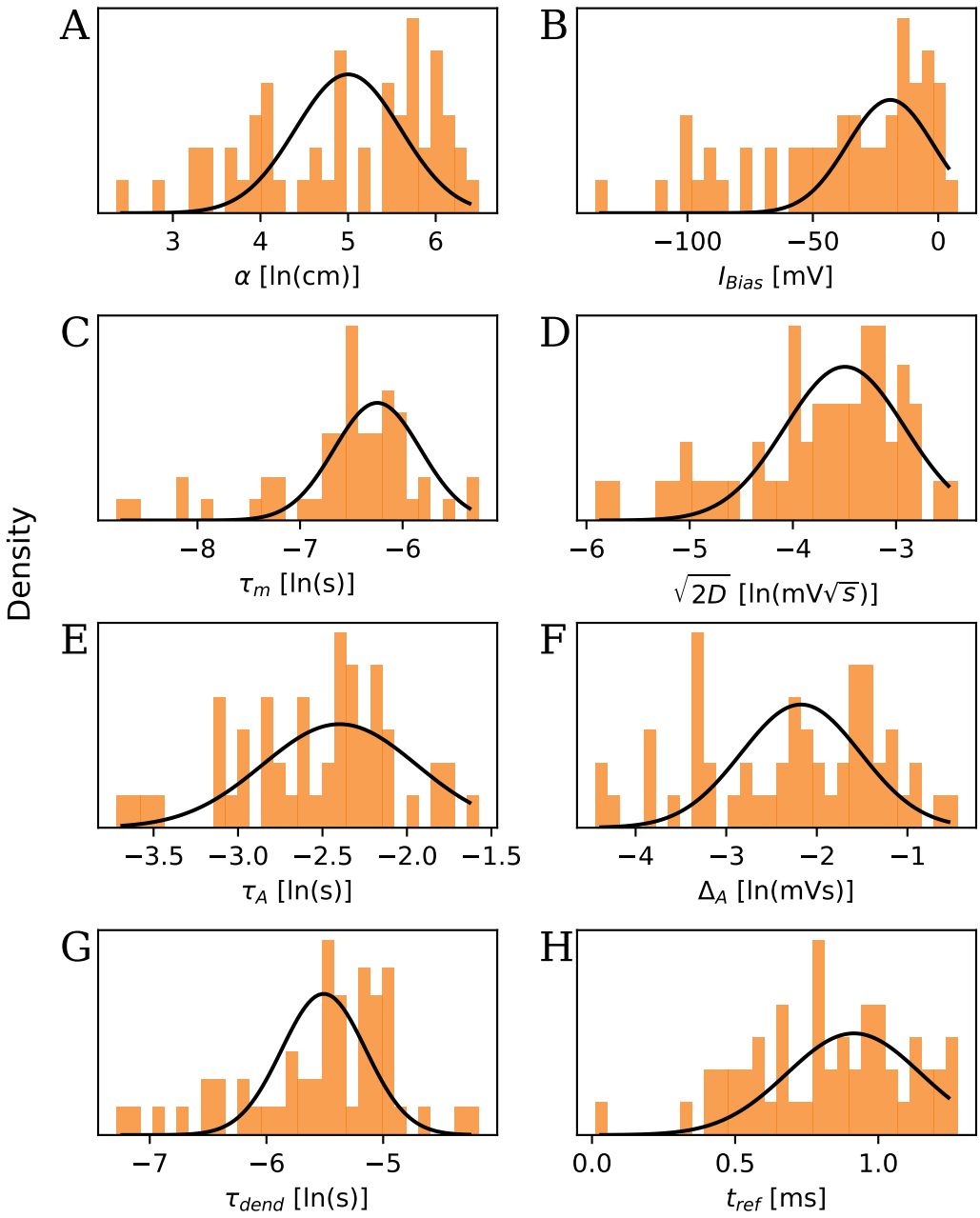

Figure 17: Gauss fits used as approximations for the parameter distribution. In black the Gaussian fit used. All parameters except for t_{ref} and I_{Bias} were log transformed to get a more Gaussian distribution. **A**: Log input scaling α, **B**: bias current I_{Bias}, **C**: Log membrane time constant τ_m, **D**: Log noise strength $\sqrt{2D}$, **E**: Log adaption time constant τ_A, **F**: Log adaption strength Δ_A, **G**: Log time constant of the dendritic low pass filter τ_{dend}, **H**: refractory period t_{ref}

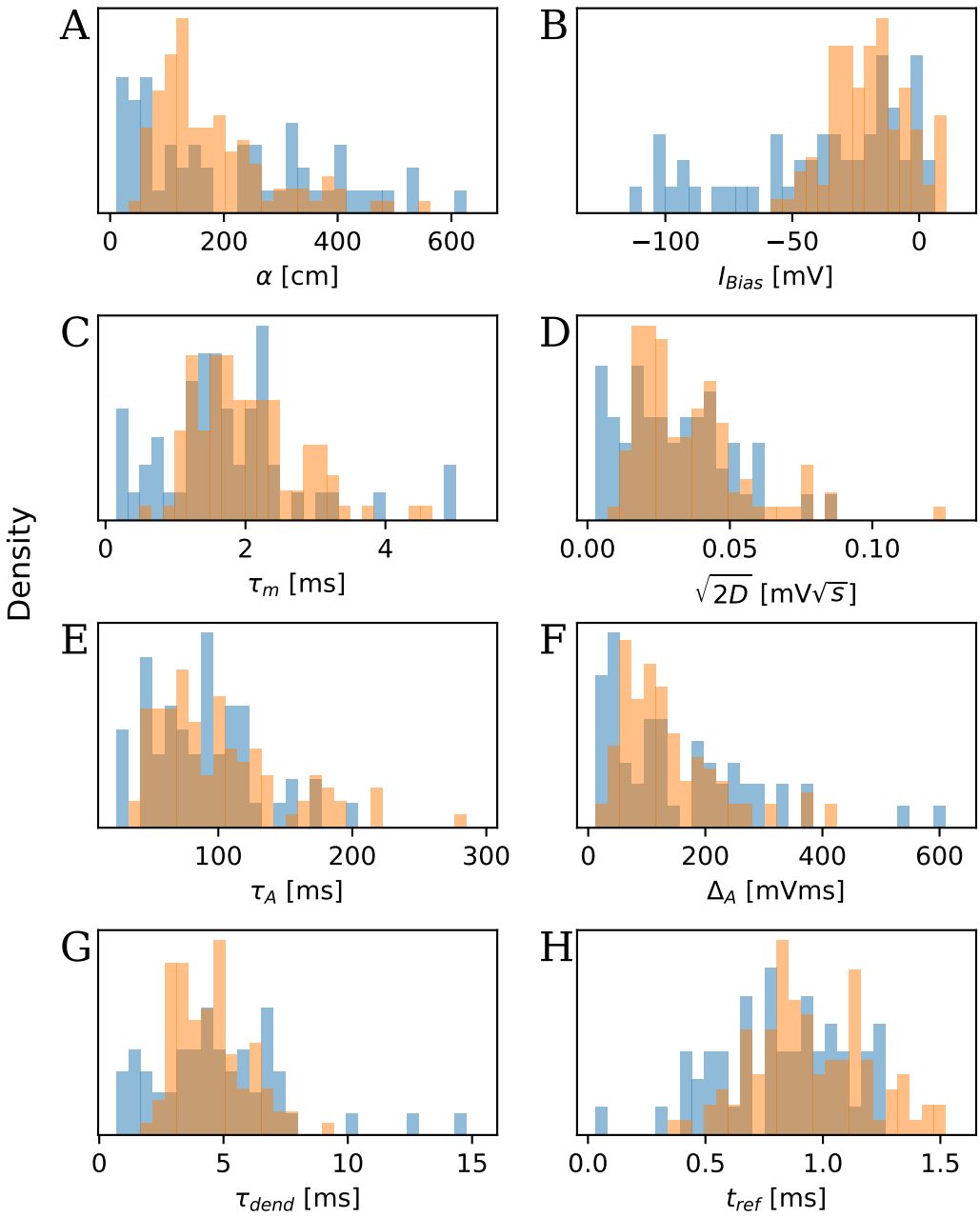

Figure 18: Parameter distribution between randomly drawn models (TODO: color)orange and the fitted ones blue(TODO: color). **A**: input scaling α, **B**: Bias current I_{Bias}, **C**: membrane time constant τ_m, **D**: noise strength $\sqrt{2D}$, **E**: adaption time constant τ_A, **F**: adaption strength Δ_A, **G**: time constant of the dendritic low pass filter τ_{dend}, **H**: refractory period t_{ref}

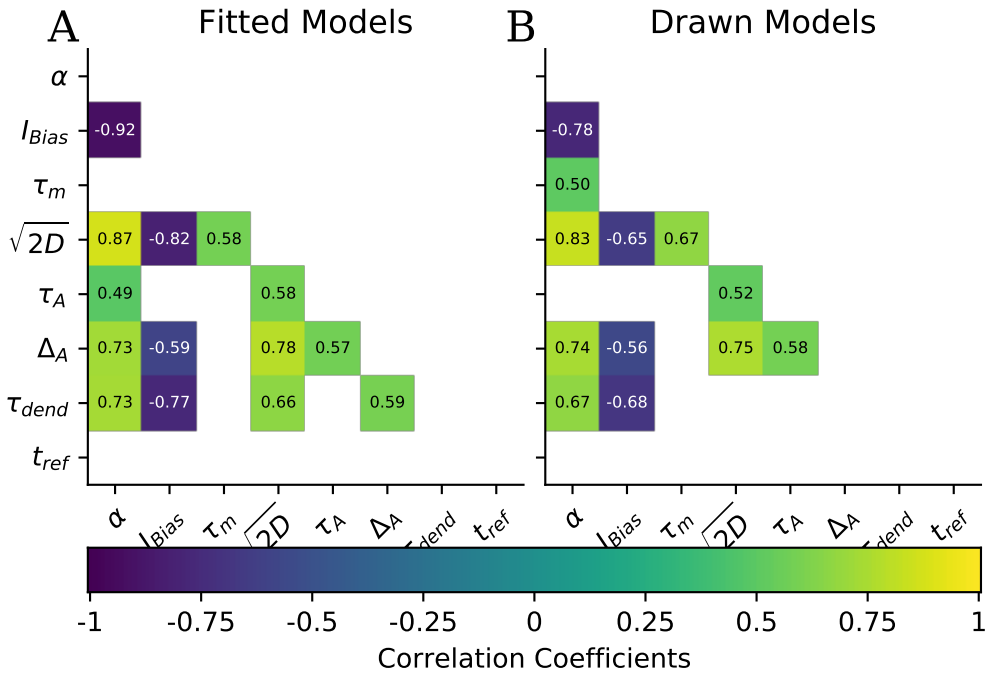

Figure 19: Parameter correlation comparison between the fitted parameters and the ones drawn from the multivariant normal distribution. There are four correlations that do not agree between the two, but those are inconsistent in the drawn models (see discussion).

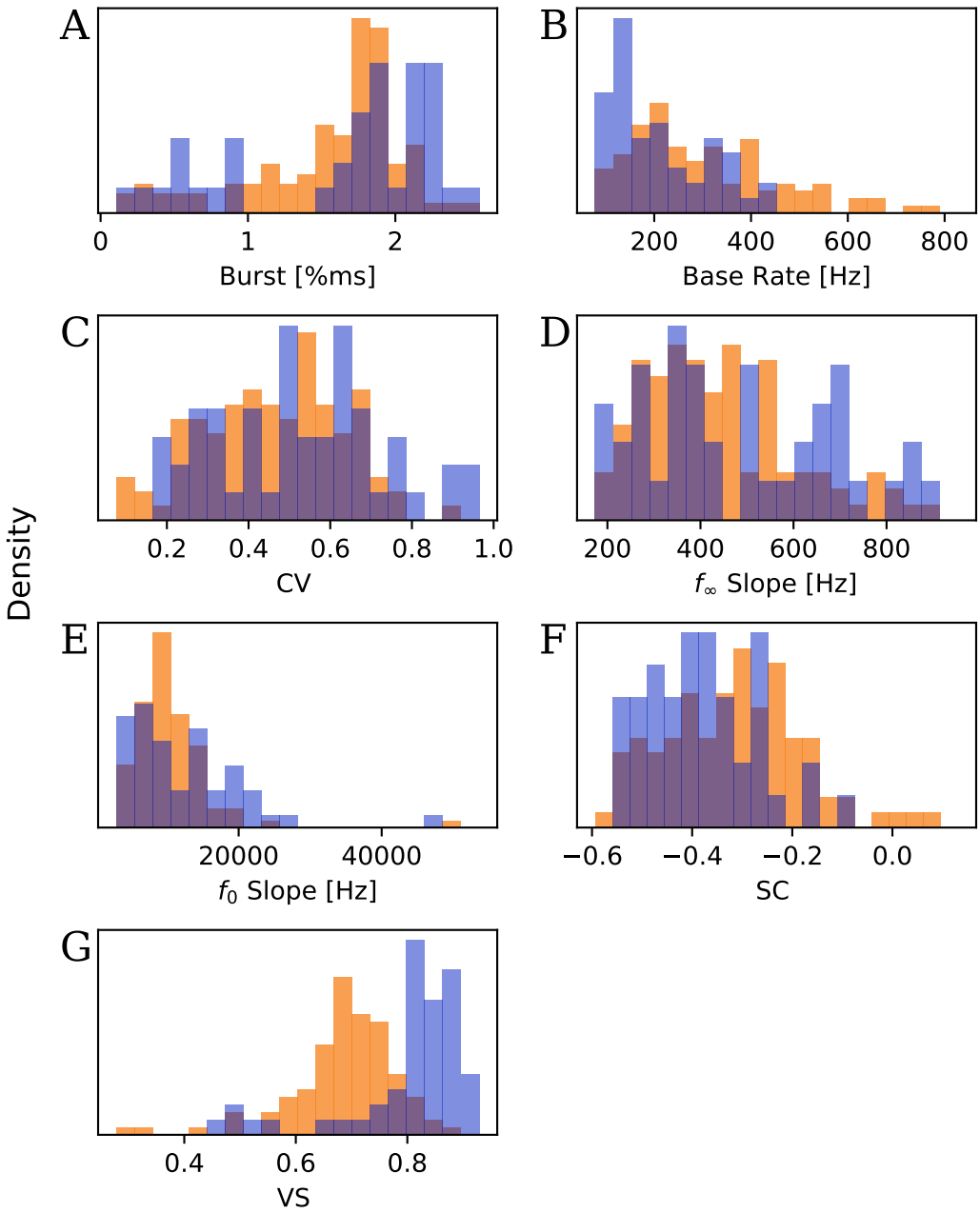

Figure 20: Behavior distribution of the randomly drawn models (TODO: color)(orange) and the original cells (TODO: color)(blue). The distribution of the seven behavior characteristics agree well for the most part, but especially the vector strength (VS) in **G** is offset to the distribution seen in the cells.

6 Discussion

In this thesis a simple model based on the leaky integrate-and-fire (LIF) model was developed to allow the simulation of a neuron population that correctly represents the heterogeneity of P-units in the electrosensory pathway of the electric fish *A. leptorhynchus*. The LIF model was extended by an adaption current, a refractory period and simulated the input synapses by rectifying and low pass filtering the input current, building on the model proposed by Walz (2013). This model was then fit to in vivo recordings of single P-units characterized by seven firing properties and the resulting models were compared to their respective reference cell. Additionally estimates of the distributions and covariances of the model parameters were used to draw random parameter sets. Simulations of these generated populations were compared with the data.

(TODO: comparison to the other already existing models)

The dendtritic low pass filter and the refractory period were necessary for the model to match the firing behavior of the P-units (fig. 7). As Walz (2013) demonstrated a model without the low pass filter is not able to match the VS and locks too strongly to the EOD. A refractory period t_{ref} is necessary for the model to deviate from the Gaussian firing probability (TODO: explain what that is) and show bursting behavior and is flexible enough to match different strengths of burstiness.

With these additions the behavior of the cells was generally matched well by the models with very similar final distributions of the firing properties but there were some limitations. The model failed to reproduce cells with a very high burstiness (long bursts with long pauses between) or a high coefficient of variation could not fully be matched by the model (TODO: burst or CV not really correct because of the correlation!). As seen in figure 12. The example of fig. 8 **A** is a case where the model can show this type firing behavior (long bursts and pauses) but it seems difficult to reach the parameter configuration needed with the fitting approach used. In contrast to that the firing behavior of the cells in fig. 8 **B** and **C** are not possible for the model in its current form. The addition of the refractory period t_{ref} does not also allow for an increased firing probability at the 2nd EOD period and the cell **C** shows a higher order structure in its ISI histogram on a comparatively long timescale which the proposed simple model cannot reproduce. These kind of cells showing higher order structure in their ISI histogram are rare but might provide interesting insights in the physiological properties of P-units when further studied.

Two firing properties had a high spread in the fitted models. In the serial correlation the models had some tendency to underestimate the cell's SC. The second property was the slope of the f_0 response. Here one possible source is that the fitted Boltzmann function and its slope are quite sensitive to miss-detections of spikes. A wrong estimate of the firing frequency for a single contrast can strongly influence the slope of the fitted Boltzmann function. Unlike the baseline firing properties there don't seem to be cases in which the model cannot fit the f-I curves. The problematic cases shown in figure 10 are both generally possible (fig. 9) so improvements in the cost function and fitting routine should also further improve the model consistency for the adaption responses.

Comparing the correlation between the firing properties of the data and the models showed clear discrepancies (fig. 14) with four additional and one missing significant correlation. The added correlation between bursts and baseline firing rate could be a result of the slightly stronger correlations between CV and base rate and between bursts and CV. The difficulties of the model to fit strongly bursting cells with a long pause between bursts could also have introduced this correlation as these cells would show high

burstiness and a low firing rate. The correlation between f_0 slope and base rate might also be caused by a slight increase in the correlations between f_∞ slope and base rate and f_∞ slope and f_0 slope. The other two added correlations are between the SC and the base rate as well as the f_∞ slope, where the former may again caused the latter because of the correlation between f_∞ and base rate. Finally the one missing correlation in the models is the one between base rate and VS, which is an unexpected correlation. This was also looked at in Walz (2013) but only 23 cells were used and they were exclusively non bursting cells which makes a direct comparison difficult. The data there showed the correlation between SC and base rate which is shown by the models in this work. This might indicate that the highest bursting cells that are not fitted well, "remove" this correlation from the population in the data or that there is not enough data to robustly define the correlation.

The parameters of the fitted models also showed extensive correlations between each other. This is an indication of strong compensation effects between them (Olypher and Calabrese, 2007). Which is especially clear for the input gain α and the bias current I_{Bias} that have a nearly perfect correlation and control the models baseline firing rate together. Note that the refractory period t_{ref} is the only completely independent variable. This might show a certain independence between the strength of the burstiness and the other firing characteristics, which could be more closely investigated by looking at the sensitivity of models firing properties to changes in t_{ref}.

The correlations and the estimated parameter distributions were used form of their covariances to draw random parameter sets from a multivariante normal distribution. The drawn parameters show the expected distributions but different correlations. That could mean that the (TODO: number) models used to calculate them were to few to give enough statistical power for the correct estimation of all correlations. Drawing more models and compensating for the increase in power showed that the involved correlations stay inconsistent, which points to an uncertainty already in the measured covariance matrix of the data. This could be further investigated with a robustness analysis estimating the reliability of the computed covariances.

The firing behavior shown by the drawn models on the other hand fits the ones of the data quite well except for the VS, where it is consistently underestimating the VS of the data.

In general the model is the first that takes the burstiness as a continuum into account and seems to be able to accurately describe the firing behavior in a large part of the behavior space of the P-units. But further testing is required to get a clearer picture where and why discrepancies exist. An important next step is the verification of the models with a different type of stimulus. For this a stimulus with random or sinusoidal amplitude modulations could be used. The correlations also need further investigation. As a first step a robustness test could be done to estimate if there are correlations that are not well characterized in both the cells and the models.

(TODO: Doesn't cover long timescales described in Gussin 2007??) (TODO: Why do we want such models - analysis of coding in heterogeneic neuron populations, possibility to "measure" responses from whole population at the same time to a single stimulus, separating the different types and analyzing their specific coding properties - finding out why the heterogeneity is necessary!)

(TODO: comparison to existing models Chacron, Waltz, Kashimori what does this model add which the others "missed" don't deliver on.)

References

Babineau, D., Lewis, J. E., and Longtin, A. (2007). Spatial acuity and prey detection in weakly electric fish. *PLoS Computational Biology*, 3(3):e38.

Barlow, H. B. et al. (1961). Possible principles underlying the transformation of sensory messages. *Sensory communication*, 1:217–234.

Bastian, J. (1981). Electrolocation. *Journal of comparative physiology*, 144(4):465–479.

Benda, J., Longtin, A., and Maler, L. (2005). Spike-frequency adaptation separates transient communication signals from background oscillations. *Journal of Neuroscience*, 25(9):2312–2321.

Benda, J., Maler, L., and Longtin, A. (2010). Linear versus nonlinear signal transmission in neuron models with adaptation currents or dynamic thresholds. *Journal of Neurophysiology*, 104(5):2806–2820.

Chacron, M. J., Longtin, A., and Maler, L. (2001). Simple models of bursting and non-bursting p-type electroreceptors. *Neurocomputing*, 38:129–139.

Gao, F. and Han, L. (2012). Implementing the nelder-mead simplex algorithm with adaptive parameters. *Computational Optimization and Applications*, 51(1):259–277.

Gussin, D., Benda, J., and Maler, L. (2007). Limits of linear rate coding of dynamic stimuli by electroreceptor afferents. *Journal of neurophysiology*, 97(4):2917–2929.

Kashimori, Y., Goto, M., and Kambara, T. (1996). Model of p-and t-electroreceptors of weakly electric fish. *Biophysical journal*, 70(6):2513–2526.

Maciver, M. A., Sharabash, N. M., and Nelson, M. E. (2001). Prey-capture behavior in gymnotid electric fish: motion analysis and effects of water conductivity. *Journal of experimental biology*, 204(3):543–557.

Olypher, A. V. and Calabrese, R. L. (2007). Using constraints on neuronal activity to reveal compensatory changes in neuronal parameters. *Journal of Neurophysiology*, 98(6):3749–3758.

Padmanabhan, K. and Urban, N. N. (2010). Intrinsic biophysical diversity decorrelates neuronal firing while increasing information content. *Nature neuroscience*, 13(10):1276–1282.

Ratnam, R. and Nelson, M. E. (2000). Nonrenewal statistics of electrosensory afferent spike trains: implications for the detection of weak sensory signals. *Journal of Neuroscience*, 20(17):6672–6683.

Scheich, H., Bullock, T. H., and Hamstra Jr, R. (1973). Coding properties of two classes of afferent nerve fibers: high-frequency electroreceptors in the electric fish, eigenmannia. *Journal of Neurophysiology*, 36(1):39–60.

Todd, B. S. and Andrews, D. C. (1999). The identification of peaks in physiological signals. *Computers and biomedical research*, 32(4):322–335.

Tripathy, S. J., Padmanabhan, K., Gerkin, R. C., and Urban, N. N. (2013). Intermediate intrinsic diversity enhances neural population coding. *Proceedings of the National Academy of Sciences*, 110(20):8248–8253.

Walz, H. (2013). *Encoding of Communication Signals in Heterogeneous Populations of-Electroreceptors*. PhD thesis, Eberhard-Karls-Universität Tübingen.

Walz, H., Grewe, J., and Benda, J. (2014). Static frequency tuning accounts for changes in neural synchrony evoked by transient communication signals. *Journal of Neurophysiology*, 112(4):752–765.

Zupanc, G., Sîrbulescu, R., Nichols, A., and Ilies, I. (2006). Electric interactions through chirping behavior in the weakly electric fish, apteronotus leptorhynchus. *Journal of Comparative Physiology A*, 192(2):159–173.